Macromolecules

Cite This: Macromolecules 2019, 52, 1241−1248

Article

pubs.acs.org/Macromolecules

Orienting Cylinder-Forming Block Copolymer Thin Films: The Combined Effect of Substrate Corrugation and Its Surface Energy

Yanyan Zhu,[†,‡] Karim Aissou,[§] David Andelman,[∥] and Xingkun Man*[,†,‡]

[†]Center of Soft Matter Physics and Its Applications and [‡]School of Physics and Nuclear Energy Engineering, Beihang University, Beijing 100191, China

[§]Institut Européen des Membranes, Université de Montpellier-CNRS-ENSCM, 300 Avenue du Professeur Emile Jeanbrau, F-34090 Montpellier, France

[∥]Raymond and Beverly Sackler School of Physics and Astronomy, Tel Aviv University, Ramat Aviv 69978, Tel Aviv, Israel

ABSTRACT: We explore the relative stability of three possible orientations of cylinder-forming diblock copolymer on a sinusoidally corrugated substrate. The cylinders can be aligned either parallel to the substrate, with their long axis being oriented along or orthogonal to the corrugation trenches, or perpendicular to the substrate. Using self-consistent field theory, we investigate the influence of substrate roughness and surface preference on the phase transition between the three orientations. When the substrate preference, u, toward one of components is small, increasing the substrate roughness induces a phase transition from parallel to perpendicular cylindrical phase. However, when u is large, the parallel orientation is more stable than the perpendicular one. Within this parallel phase, increasing the substrate roughness leads to a transition of the cylinder orientation changing from being orthogonal to parallel to the trench long axis. Increasing the substrate preference leads to an opposite transition from parallel to orthogonal to the trenches. Furthermore, we predict that the perpendicular cylindrical phase is easier to be obtained when the unidirectional corrugation is along the longer unit vector of the hexagonal packing than when it is along the shorter unit vector. Our results qualitatively agree with previous experiments and contribute toward applications of the cylinder-forming block copolymer in nanotechnology.

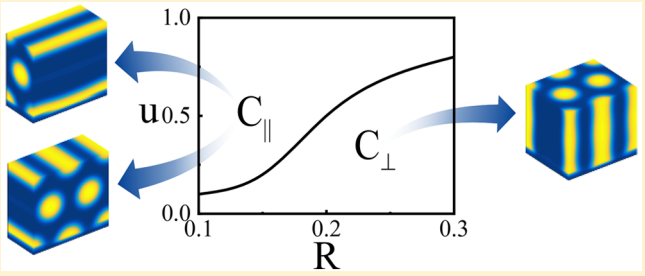

I. INTRODUCTION

Block copolymers (BCPs) are composed of two or more chemically distinct blocks, which are covalently bonded together. The chemical incompatibility between the different blocks drives a microphase separation, in which the BCP can form a variety of well-ordered nanostructures via self-assembly. The phase behavior of BCP melts has been studied extensively in recent years, showing a rich variety of morphologies, such as lamellae, hexagonally close-packed (HCP) cylinders, body-centered cubic (BCC) packing of spheres, and complex networks such as the cubic double gyroid (Q^{230}) and orthorhombic O^{70} phases.[1−4] The length scale of microphase separation is in the range 10−100 nm, making them ideal for emerging nanotechnologies,[5] including applications in nano-lithography,[6,7] nanoporous membranes,[8] and magnetic nano-wires.[9,10]

In many cases, capturing the vast technological potential of BCP thin film requires precise control over the orientation and the lateral alignment of these nanostructures to produce defect-free array of BCP features. In recent decades, much effort has been devoted to tailor the self-assembly behavior of BCP thin films by using engineering surface effects,[11,12] external fields,[13] patterned substrates,[14−17] and solvent vapor annealing.[18] Among these approaches, the use of nonflat substrates to direct the self-assembly of BCP thin films has been proven to be an effective method to achieve long-range ordered arrays with either a parallel or perpendicular orientation of BCP domains with respect to the substrate.

When BCP lamellae or cylinders are parallel to the unidirectional corrugated substrate, the domain orientation can be orthogonal, parallel, or aligned with a tilted angle with respect to the trench long axis. Previous experimental studies have shown that the film thickness,[19−21] substrate mean curvature,[15] and roughness and chemical preference of the substrate[22] are key factors in determining the orientation of BCP domains with respect to the trenches.

A large lateral scale and nearly defect-free cylindrical BCP thin films, which are perpendicular to the substrate, were obtained from various types of nonflat substrates, such as sawtoothed topography,[23] sinusoidal pattern,[24,25] ordered nanoparticle monolayers,[26] minimal topographic pattern,[27] and so forth. To the best of our knowledge, only Kim et al.[26] and Aissou et al.[28] investigated experimentally the transition of cylinder orientation from parallel to perpendicular with respect to the nonflat substrate. They showed that this transition can

Received: October 26, 2018
Revised: January 8, 2019
Published: January 30, 2019

DOI: 10.1021/acs.macromol.8b02302
Macromolecules 2019, 52, 1241−1248

be obtained either by increasing the substrate roughness[26] or by decreasing the film thickness.[28]

In view of the above-mentioned experimental studies, there are only a few theoretical works addressing the self-assembly of BCP films on corrugated surfaces. Peng et al.[29] employed self-consistent field theory (SCFT) to explore the self-assemble behavior of cylinder-forming BCP thin films on a sawtoothed substrate. They investigated the effects of the substrate corrugation periodicity and the film thickness on cylindrical structures. Man et al.[30,31] systematically studied the self-assembly of lamellar forming BCP thin film on a sinusoidal substrate and showed an enhanced synergy between substrate topography combined with a weak surface preference to produce defect-free perpendicular lamellar BCP thin films. Recently, Carpenter et al.[32] presented a study combining SCFT calculations with experimental results and found that the orientation of cylinders with respect to the trench depends on the commensurability of the hexagonal packing of the BCP features with the substrate characteristic length and the film thickness.

Aforementioned studies[29] show that when cylinder forming BCP self-assembly on an unidirectional corrugated substrate, there are three possible orthogonal cylinder orientations. The cylinders can be either perpendicular or parallel to the substrate, while the latter one can be characterized by a tilted angle with respect to the trench long axis. Previous studies[21,28] showed that varying the substrate roughness and the film thickness can cause phase transitions between these orientations. In spite of this progress, a quantitative mechanistic understanding of the effect of nonflat substrate in determining the cylinder orientation in BCP thin films is still missing. Here, we investigate the self-assembly of cylinder-forming di-BCP thin films on a sinusoidally corrugated substrate. By use of SCFT, our aim is to explain the effects of substrate geometry and relative surface preference to one of the di-BCP components on the transition between the three cylinder orientations.

This paper is organized as follows. In the next section, we introduce the self-consistent field theory (SCFT) technique and our model. In section III, we present the phase diagram of BCP cylinder on corrugated substrates, followed by the discussion of our results, conclusions and some future prospects in section IV.

II. MODEL

We employ self-consistent field theory (SCFT) to investigate the self-assembly of cylinder-forming block copolymer thin film. The BCP thin film is confined between a flat top surface and a sinusoidally corrugated bottom one, as shown in Figure 1a. Specifically, we describe the polymer as a Gaussian chain composed of N segments, of which a fraction f are of type A and $(1 - f)$ of type B. The interactions between A and B monomers are mediated through the Flory parameter χ_{AB}, and $u = N\chi_{sA} - N\chi_{sB}$ is the relative interaction between the substrate and the A (B) component, where χ_{sA} (χ_{sB}) is the interaction parameter between the substrate and the A (B) component. This choice means that $u > 0$ induces substrate preference of the A component. We model the periodic surface trenches by a single q-mode along the x-direction with periodicity L_s and amplitude R, $h(x) = R\cos(2\pi x/L_s)$. Lateral confinement is modeled by the masking method, where the wall is described as the third component.[33] The wall volume fraction, $\phi_w(\mathbf{r})$, has a preassigned shape that is fixed during the iterations. The top flat wall is modeled as a box of size $L_x \times L_y \times L_z$ and is characterized by a smoothly varying wall function:

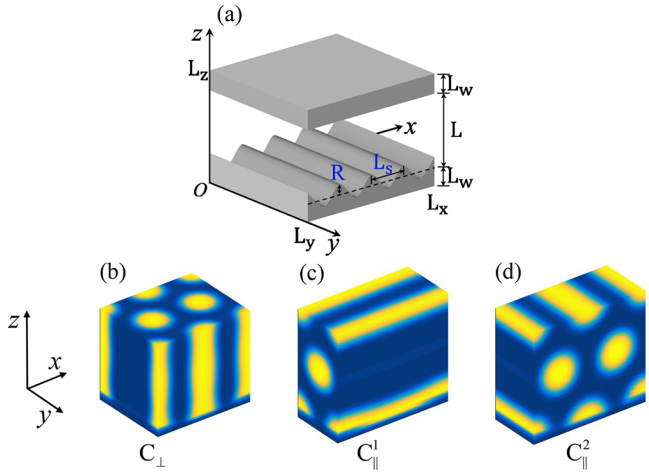

Figure 1. Schematic illustration of a BCP film confined between two surfaces and its cylinder orientations for a bottom substrate that is sinusoidally corrugated. The size of the 3D calculation box is $L_x \times L_y \times L_z$. (a) The averaged BCP film thickness is $L = L_z - 2L_w$, where L_w is the average wall thickness within the box. The substrate corrugation describes trenches that are translationally invariant in the y-direction with periodicity L_s and amplitude R, $h(x) = R\cos(2\pi x/L_s)$. A-rich regions are denoted by yellow and B-rich by blue. In (b), the cylinder orientation is perpendicular to the substrate, and the phase is denoted as $C_\perp$, while in (c) and (d) we show the two orientations that are parallel to the substrate (and orthogonal to each other). In (c), the cylinders are perpendicular to the long axis of the substrate trenches, and the phase is denoted as $C_\parallel^1$. In (d), the cylinders are parallel to the trench long-axis, and the phase is denoted as $C_\parallel^2$.

$$\phi_w(\mathbf{r}) = \frac{1}{2} + \frac{1}{2}\tanh\left(\frac{z - L_w - L}{\delta}\right) \tag{1}$$

where L is the average BCP film thickness, L_w is the average wall thickness, and δ is used to set the interface width. For the bottom sinusoidal substrate, we impose a similar smoothly varying wall function:

$$\phi_w(\mathbf{r}) = \frac{1}{2} - \frac{1}{2}\tanh\left(\frac{z - R\cos(q_s x) - L_w}{\delta}\right) \tag{2}$$

Such a definition means that $\phi_w(r) = 1$ for the wall region and $\phi_w(r) = 0$ for the BCP film. All lengths are rescaled with the chain radius of gyration, $R_g = \sqrt{Nb^2/6}$, where b is the Kuhn length taken for simplicity to be the same for the two blocks.

The Hamiltonian for a di-BCP film confined between the two surfaces can be expressed as a functional of two conjugate potential fields, $W_+(x)$ and $W_-(x)$:

$$H[W_+, W_-] = C\int d^3\mathbf{r}\left(\frac{[W_-(\mathbf{r})]^2}{N\chi_{AB}} - \frac{2Nu}{N\chi_{AB}}\phi_w(\mathbf{r})W_-(\mathbf{r}) + \frac{[W_+(\mathbf{r})]^2 - 2\zeta N\phi_p(\mathbf{r})iW_+(\mathbf{r})}{N\chi_{AB} + 2N\zeta}\right) - C\Omega\overline{\phi_p}\ln Q[W_A, W_B] \tag{3}$$

DOI: 10.1021/acs.macromol.8b02302
Macromolecules 2019, 52, 1241−1248

where $C = \rho_0 R_g^3/N$ is a normalization factor. The total volume of the simulation box is Ω, and $\phi_w + \phi_p = 1$, ϕ_w is the wall volume fractions, and $\phi_p(\mathbf{r})$ is the dimensionless volume fraction of the polymer, $\phi_p(\mathbf{r}) = \phi_A(\mathbf{r}) + \phi_B(\mathbf{r})$. $\overline{\phi}_p = \Omega^{-1}\int d^3\mathbf{r}\, \phi_p(\mathbf{r})$ is the polymer volume fraction averaged over Ω. In addition, ζ is a penalty cost for local density deviation from the incompressibility condition, and $Q[W_A,W_B] = \Omega^{-1}\int d^3\mathbf{r}\, q(\mathbf{r}, s{=}1)$ is the single-chain partition function for BCP, in which the propagator $q(\mathbf{r}, s)$ is the solution of the following modified diffusion equation:

$$\frac{\partial q(\mathbf{r}, s)}{\partial s} = \nabla^2 q(\mathbf{r}, s) - W(\mathbf{r}, s) q(\mathbf{r}, s) \tag{4}$$

where $W(\mathbf{r}) = W_A(\mathbf{r})$ for $0 \le s < f$ and $W(\mathbf{r}) = W_B(\mathbf{r})$ for $f \le s \le 1$. The initial condition for eq 4 is $q(\mathbf{r}, s) = 1$.

In the mean-field approximation, the thermodynamic properties of the confined melt can be obtained from saddle-point configurations of the Hamiltonian in eq 3, i.e., solutions of

$$\frac{\delta H[W_+, W_-]}{\delta(iW_+(\mathbf{r}))} = \frac{\delta H[W_+, W_-]}{\delta(W_-(\mathbf{r}))} = 0 \tag{5}$$

A detailed formulation of the numerical procedure and its implementation to SCFT modeling of BCP systems can be found elsewhere.[34−36]

The SCFT formulation gives the local density for the A and B components, $\phi_A(\mathbf{r})$ and $\phi_B(\mathbf{r})$, respectively. There are three orientations of the cylindrical phase with respect to the substrate, as shown schematically in Figure 1. The perpendicular orientation is denoted $C_\perp$ (see Figure 1b), while the parallel orientation can be divided into two orientations, $C_\parallel^1$ and $C_\parallel^2$, which are orthogonal to each other, as well as to the $C_\perp$, as shown in Figures 1c,d. Whereas $C_\parallel^1$ is orthogonal to the trench long axis, the $C_\parallel^2$ ordering is oriented along the trench direction. The BCP film is in contact with a unidirectional corrugated substrate, which has a preference toward one of the two BCP components.

From the characteristics of the hexagonal phases as shown in Figure 2, it is evident that a unidirectional corrugated substrate undulate not only along the short (a-direction) but also along the long (b-direction) unit vectors. Therefore, we present hereafter the effect of the substrate on the cylindrical phase in both cases and the corresponding phase diagram of the three orientations.

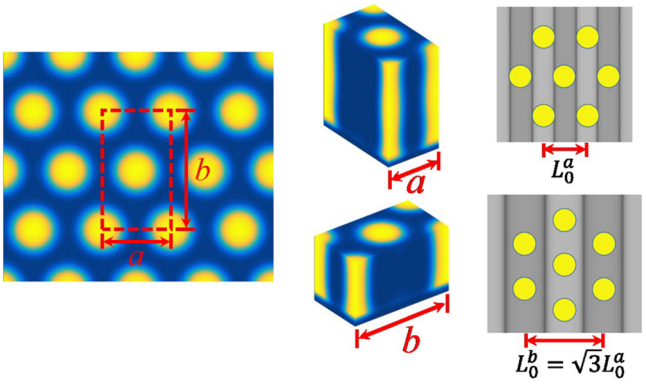

Figure 2. Schematic drawing (top view) of the hexagonally close-packed cylindrical phase (left). The two directions, labeled as a and b, indicate the short and long unit vectors of the hexagonal unit cell, respectively. The unidirectional corrugated substrate undulates along the a-direction or the b-direction of the cylindrical phase, as shown in the middle of the figure. The right two figures are the top view of the two different undulation cases.

III. RESULTS

We focus on the effects of sinusoidal substrates on the orientation of a confined BCP cylindrical phase. The segregation strength is fixed at $N\chi_{AB} = 25$, and the fraction of minority A component is $f = 0.3$. For these values, the behavior falls well within the cylindrical region of the bulk phase diagram.[37] For this $N\chi_{AB}$ value, the characteristic BCP lengths in a thin film geometry are $L_0^a = 4.4$ and $L_0^b = \sqrt{3}L_0^a = 7.6$ (in units of R_g). These values are obtained by varying the film thickness and comparing the corresponding free energies to find at which thickness the free energy has a minimum. We set the average film thickness to be an integer number of L_0^b (L_0^a) to limit the z-direction space confinement effects on the cylinder orientation when the unidirectional corrugation is along the a-direction (b-direction). The top surface is always flat and neutral ($u_{top} = 0$). The orientation of the cylindrical phase in the BCP thin film mainly depends on the substrate roughness whose height, $h(x) = R\cos(2\pi x/L_s)$, is described by the corrugation periodicity L_s and amplitude R. The strength of substrate preference toward one of the two components is u and is chosen to be a positive when the substrate prefers the minority A component.

Figure 3 shows various deformed BCP cylindrical phases due to either large substrate roughness or strong substrate preference. For deformed cylindrical phases, it is hard to recognize which orientation is the equilibrium structure. Therefore, we limit ourselves to a range of parameters resulting in perfect BCP cylindrical phase. Figure 3a is a deformed $C_\perp$ phase on a neutral substrate with $L_s = 2L_0^a$ and $R = 0.3$. We find that when $L_s \le 2L_0^a$, it is difficult to obtain perfect cylindrical phase even when R is reasonably small. Furthermore, the value of R cannot be too large; otherwise, $C_\perp$ is deformed as shown in Figure 3b. Numerical calculations show that $R < 0.4$ for

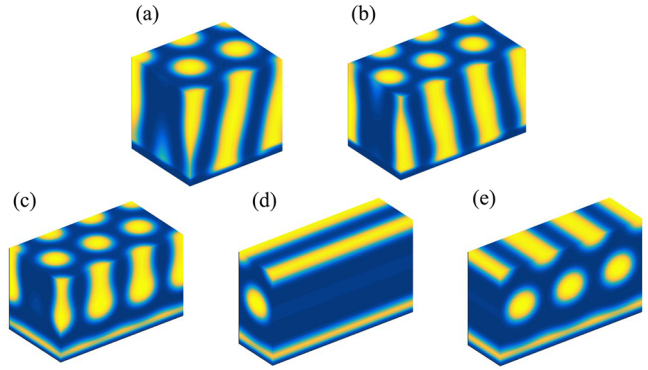

Figure 3. SCFT calculation of BCP cylindrical phase in contact with a substrate, of which its undulation is along the a-direction for, small L_s in (a), large R in (b), and large u in (c−e). For (a), the corrugation periodicity is $L_s = 2L_0$ and its amplitude $R = 0.3$, leading to a deformed perpendicular cylindrical phase, $C_\perp$. For (b), the substrate parameters are $L_s = 3L_0$ and $R = 0.4$, also resulting in a deformed $C_\perp$. In both (a) and (b), the top and bottom surfaces are neutral. Strong substrate preference results in deformed cylindrical phases for all three orientations ($C_\perp$, $C_\parallel^1$, and $C_\parallel^2$), as shown in (c), (d), and (e), respectively, and the other parameters are $R = 0$ and $u = 9$.

DOI: 10.1021/acs.macromol.8b02302
Macromolecules 2019, 52, 1241−1248

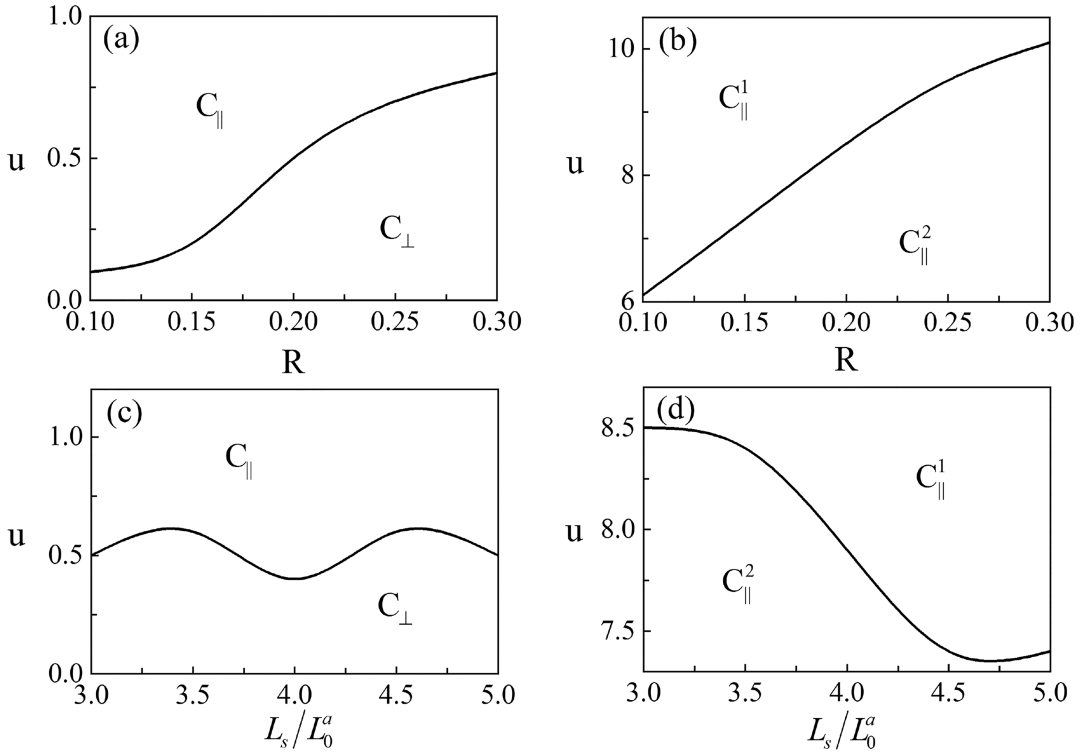

Figure 4. $C_\perp$-to-$C_\parallel$ and $C_\parallel^2$-to-$C_\parallel^1$ phase transitions in terms of the substrate roughness parameter: the amplitude R, the ratio L_s/L_0, and the preference u. The lines separate the parallel orientations above from the perpendicular orientation below. (a) The $C_\perp$−$C_\parallel$ phase transition in the (R, u) plane. (b) The phase transition of the two parallel orientations, separating the $C_\parallel^1$ above from $C_\parallel^2$ below. In both (a) and (b), $L_s = 3L_0^a$. (c) and (d) show the same phase diagrams as in (a) and (b), separately, but for the (L_s/L_0, u) plane, where the substrate roughness is varied by changing L_s while keeping $R = 0.2$. For all cases, the top flat surface is neutral, $N\chi_{AB} = 25$ and $L_0^a = 4.4R_g$.

$L_s = 3L_0^a$ and for $u = 0$ to avoid such deformations. Besides the substrate roughness, the strength of the substrate preference, u, can also induce deformed cylindrical phases. Figures 3c−e show that $u = 9$ is already large enough to generate a wetting layer of A component along the substrate surface. Therefore, all our simulations were conducted within the parameter range of $R < 0.4$, $L_s \geq 3L_0$, and $|u| \leq 9$.

Unidirectional Substrate Corrugation along the *a*-Direction. The unit cell of the cylindrical phase is composed of two unit vectors: a short one, L_0^a, and the long one, L_0^b. The effects of nonflat substrate on the relative stability of the cylindrical phase with three orthogonal orientations ($C_\perp$, $C_\parallel^1$, and $C_\parallel^2$) will be different when the substrate unidirectional corrugation undulates along the *a*- or *b*-direction. This is due to the fact that the distortion effects of nonflat substrates on the BCP cylinders mainly depends on the ratio between the periodicity of sinusoidal substrate and the cylinder characteristic lengths.

We start with the corrugation along the *a*-direction and study quantitatively the effect of corrugated substrate on the phase transition between the three orientations. We focus on the role played by (i) the substrate roughness that is described by lateral variational periodicity L_s and roughness amplitude R and (ii) the relative surface preference toward the BCP components, u.

Figure 4 shows the phase transition between the perpendicular and parallel orientations ($C_\perp$-to-$C_\parallel$) and between the two parallel orientations themselves ($C_\parallel^2$-to-$C_\parallel^1$) in terms of the substrate roughness, $2\pi R/L_s$, and the substrate preference, u. In previous studies,[30] it has been shown that there are two ways to change the substrate roughness. First, we fix the corrugation periodicity, L_s, to $3L_0^a$ and then change the amplitude R from 0.1 to 0.3, as shown in Figures 4a,b. Alternatively, we present in Figures 4c,d the cases where L_s/L_0^a varies from 3 to 5 while keeping $R = 0.2$. For both cases, the effects of a weak substrate preference (small u) and a strong substrate preference (large u) on the BCP phase transitions were separately investigated. The top surface is always taken to be a neutral surface.

The substrate preference makes the parallel orientation more stable than the perpendicular one. Therefore, increasing u results in a $C_\perp$-to-$C_\parallel$ phase transition as shown in Figures 4a,c. Here, $C_\parallel$ includes both $C_\parallel^1$ and $C_\parallel^2$. It is interesting to note that when u becomes large (see Figures 4b,d), the $C_\parallel^2$-to-$C_\parallel^1$ transition is obtained, indicating that $C_\parallel^1$ is more stable than $C_\parallel^2$ when the substrate preference is strong. The critical u value that is needed to induce both the $C_\perp$-to-$C_\parallel$ and $C_\parallel^2$-to-$C_\parallel^1$ transitions increases as a function of the substrate roughness (see Figures 4a,b,d). However, the critical u value oscillates when R is fixed and $L_s/L_0^a = 3$, 3.5, 4, 4.5, and 5 as shown in Figure 4c. For weak surface preferences, Figure 4c also shows the critical u value becomes smaller when L_s/L_0^a is an integer number as compared with half-integer values of L_s/L_0^a. This phenomenon is due to the fact that the lattice distortion of parallel oriented cylinders is smaller in the former case which locally increases the stability range of the $C_\parallel$ phase over the $C_\perp$ one. For strong u preferences, the substrate preference dominates the relative stability of the two parallel orientations. Therefore, u is a monotonically increasing function of the substrate roughness, as shown in Figures 4b,d.

To understand the effects of nonflat substrates on the relative stability of the three orientations, $C_\parallel^1$, $C_\parallel^2$, and $C_\perp$, we

DOI: 10.1021/acs.macromol.8b02302
Macromolecules 2019, 52, 1241−1248

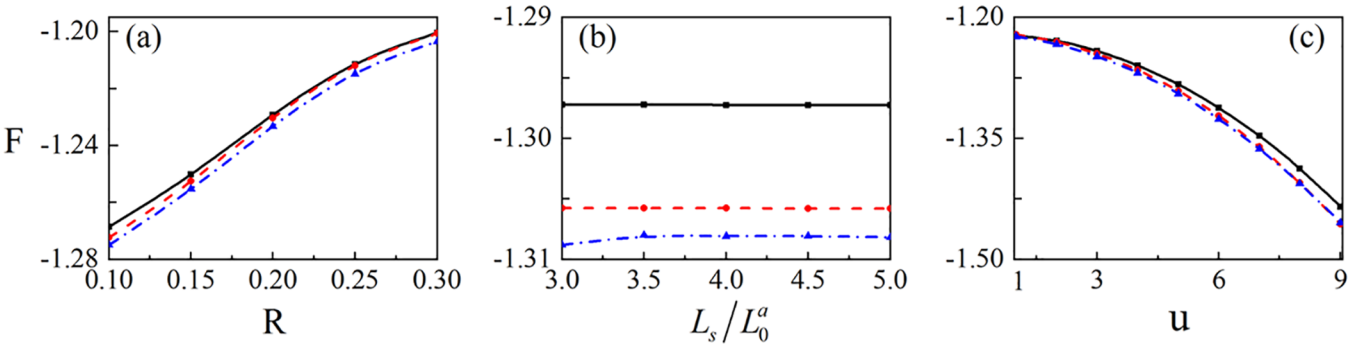

Figure 5. Dependence of the free energy for the three orientations $C_\perp$ (black line), $C_\parallel^1$ (red line), and $C_\parallel^2$ (blue line) on (a) substrate corrugation amplitude, R, (b) rescaled substrate lateral corrugation periodicity, L_s/L_0^a, and (c) substrate preference, u. The top surface is neutral, $u_{top} = 0$ and $N\chi_{AB} = 25$, and the unidirectional substrate corrugation is along the a-direction.

study the dependence of their corresponding free energy on R, L_s, and u. In Figure 5a, $u = 2$ and all other parameters are the same as in Figure 4b. It is clear that the free energies for the three orientations increase as R increases due to the increase of substrate roughness. Moreover, the two parallel orientations, $C_\parallel^1$ and $C_\parallel^2$, are more stable than the perpendicular orientation because of the surface preference. On the other hand, all free energies are nearly unchanged when L_s increases, as shown in Figure 5b for $u = 2$ and $R = 0.2$. This occurs only because we scan a limited L_s range $3 \le L_s/L_0^a \le 5$ to avoid deformations of the cylindrical phase (as in Figure 3). It is also found that the stability range of $C_\parallel^2$ is larger than that of $C_\parallel^1$ and $C_\perp$, and the latter $C_\perp$ phase is the most unstable one. These results agree with the phase diagram shown in Figures 4b,d.

The dependence of the free energy on the surface u preference is shown in Figure 5c, where calculations are done for $R = 0.2$, $L_s/L_0^a = 3$, and a neutral top surface. For the three cases, the free energy decreases as u increases, and both $C_\parallel^1$ and $C_\parallel^2$ orientations free energies decrease faster than the perpendicular one. This is consistent with the results shown in Figure 4 and also in previous studies.[22,30,31]

Unidirectional Substrate Corrugation along the *b*-Direction. Hereafter, we investigate the same phase diagram as in Figure 4, but with the substrate corrugation now along the b-direction. We scan a smaller range of the R and L_s parameters because the characteristic length, $L_0^b = \sqrt{3}L_0^a = 7.6$, is larger than L_0^a in the a-direction. To have L_s/L_0^b large enough to maintain a perfect cylindrical phase ($L_s/L_0^b \ge 3$), the size of the calculation box in the x-direction should be much larger than those presented in Figure 4 for the same ratio. Consequently, we take three values of $L_s/L_0^b = 3$, 3.5, and 4 for constant $R = 0.2$, and for a fixed value $L_s = 3L_0^b$ and $R = 0.1$, 0.15, and 0.2.

A comparison of the phase diagram of $C_\perp$–$C_\parallel$ and $C_\parallel^2$–$C_\parallel^1$ for the two different corrugation directions is presented in Figure 6, where the solid and dashed lines correspond to the corrugation along the a- and b-directions, respectively. The critical value of u needed to induce the $C_\perp$-to-$C_\parallel$ transition is much larger for the corrugation along the b-direction than along the a-direction, regardless of the substrate roughness values (by varying either R or L_s) (see Figures 6a,b). Our result indicates that the perpendicular orientation is more stable when it is in contact with a unidirectional substrate corrugation along the b-direction rather than along the a-direction. We further note that the behavior of the $C_\parallel^2$-to-$C_\parallel^1$ transition in terms of the substrate roughness and preference u is nearly the same for both the a- and b-substrate corrugation directions. The transition between the $C_\parallel^1$ and $C_\parallel^2$ phases takes place only when u, the substrate preference, is strong. Therefore, the relative stability of the two parallel orientations is mainly dominated by the substrate preference and not by the substrate roughness.

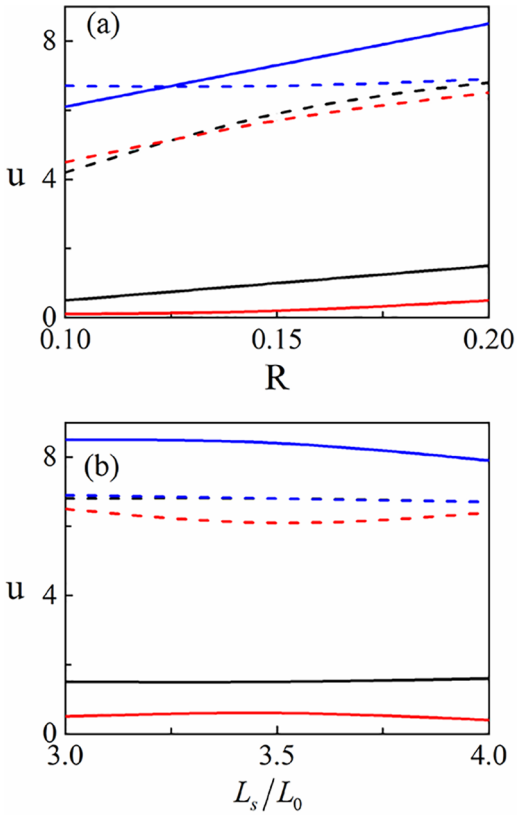

Figure 6. Comparison of the relative stability of the three orientations ($C_\perp$, $C_\parallel^1$, and $C_\parallel^2$). The substrate corrugation along the a- and b-directions are represented as the solid and dashed lines, respectively. The black (red) lines denote the critical values between $C_\perp$ and $C_\parallel^1$ ($C_\parallel^2$), while the blue lines indicate the transition between two parallel phases. (a) Phase diagrams in the (R, u) plane for $L_s = 3L_0^a$. (b) Phase diagrams in the (L_s/L_0, u) plane for $R = 0.2$. The top surface is neutral for both cases.

Although the substrate corrugation direction has a large effect on the relative stability of parallel and perpendicular cylinders, the corresponding free energy dependence on R and u is quite similar. Figure 7 shows that the free energy of the

DOI: 10.1021/acs.macromol.8b02302
Macromolecules 2019, 52, 1241−1248

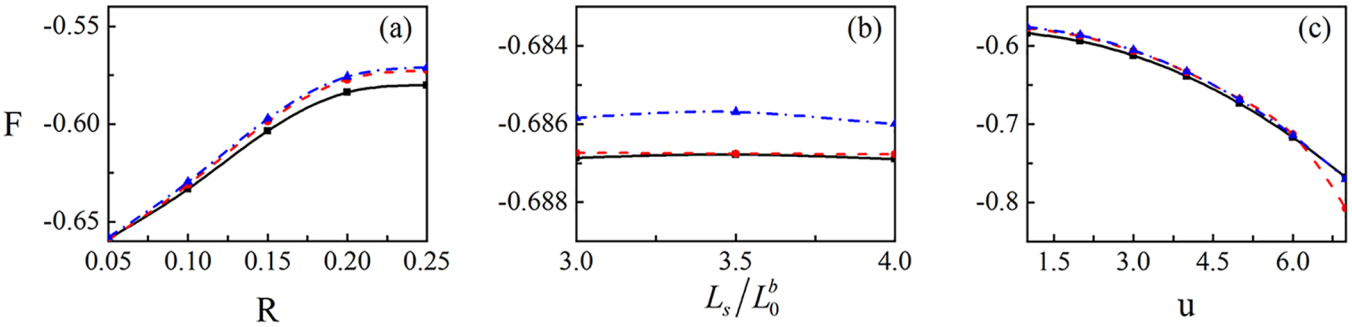

Figure 7. Dependence of the free energy for the three orientations: $C_\perp$ (black line), $C_\parallel^1$ (red line), and $C_\parallel^2$ (blue line) on (a) substrate corrugation amplitude R; (b) rescaled substrate lateral corrugation periodicity L_s/L_0^b; and (c) substrate preference u for the unidirectional substrate corrugation along the b-direction. The top surface is neutral and $N\chi_{AB} = 25$.

three orientations increases as a function of R but decreases with u. Moreover, the free energy nearly remains unchanged when L_s/L_0^b changes from 3 to 4, in analogy with the corrugations along the a-direction.

IV. DISCUSSION AND CONCLUSIONS

We explore how nonflat substrates affect the relative stability between the three orientations, $C_\perp$, $C_\parallel^1$, and $C_\parallel^2$, of BCP cylindrical phases. In general, when u is small, increasing the substrate roughness will enhance the compression of the parallel cylinders because the polymers stand perpendicularly with respect to the substrate. Therefore, the perpendicular cylindrical phase becomes more stable than the $C_\parallel$ phase due to the fact that the polymeric chains are lying down and feel less compression within the $C_\perp$ phase. For large u, $C_\parallel$ becomes more stable than $C_\perp$ because the substrate has a strong preference to the A-block. In the $C_\parallel$ stable region of the phase diagram, increasing the substrate roughness causes a transition from $C_\parallel^1$ to $C_\parallel^2$. This happens because the corrugation causes larger distortion to the $C_\parallel^1$ phase than to the $C_\parallel^2$ one. The former one aligns orthogonally to the trenches, while the latter one aligns along with the trenches. Moreover, increasing u leads to a transition from the $C_\parallel^2$ phase to the $C_\parallel^1$ one. Here, the contact area of the A component with the substrate in the $C_\parallel^1$ phase is the largest among the three phases.

Corrugated substrates affect differently on the relative stability between $C_\perp$ and $C_\parallel$ when the corrugation is along the a- or b-direction. For both cases, the cylinder characteristic lengths are $L_0^a = 4.4R_g$ and $L_0^b = \sqrt{3}L_0^a$. Figure 2 indicates that for a fixed ratio of L_s/L_0^a and L_s/L_0^b with same amplitude, R, the packing frustration of the perpendicular cylindrical phase is smaller when the substrate undulated along the b-direction than along the a-direction because of the longer characteristic length of the b-direction, resulting in a smaller substrate roughness. In this situation, the relative stability of $C_\perp$ to $C_\parallel$ on a sinusoidal substrate with b-direction undulation becomes larger than with a-direction undulation, which is also confirmed by the free energy calculations shown in Figures 5a and 7a. Therefore, a larger value of u is needed to cause the orientation transition from $C_\perp$ to $C_\parallel$, as indicated by the solid and dashed black and red lines in Figures 6a,b. Meanwhile, Figures 4b,d show that the phase transition between $C_\parallel^1$ and $C_\parallel^2$ happens only when the substrate preference is strong ($u \geq 6$). Because of the fact that calculations only scan a limited range of substrate roughness, the two parallel phase transition behavior is dominated by the substrate preference rather than its roughness. This is why the sinusoidal substrate roughness-induced transition between the two parallel phases is nearly the same when the undulation is in either of the two directions, as indicated by the solid and dashed blue lines in Figures 6a,b.

We can obtain a stable perpendicular cylindrical phase by varying the substrate roughness parameters R or L_s. As shown in Figure 4a, increasing R causes the perpendicular orientation to become more stable for $R < 0.4$, $L_s = 3L_0^a$ and $|u| \leq 1$. This observation agrees well with the Kim et al. experiment.[26] They investigate the domain orientation of thin films of polystyrene-*block*-poly(methyl methacrylate) (PS-*b*-PMMA) placed on manolayer of ordered nanoparticle (NP). Here the NP monolayers consisted of closely packed NPs with an average diameter of 6 and 22 nm, resulting in different substrate roughness parameters, q_sR, of 4.5 and 5.72, respectively. For such kinds of surfaces, a transition from the parallel to perpendicular orientation is obtained by increasing the substrate roughness (i.e., by changing the NP diameter from 6 to 22 nm). We find the same tendency that increasing the substrate roughness q_sR from 0.05 to 0.14 causes a parallel to perpendicular orientation transition ($C_\parallel^2$-to-$C_\perp$).

In addition, Aissou et al.[28] reported that the domain orientation can be controlled by tuning the layer thickness of poly(1,1-dimethylsilabutane)-*b*-PMMA (PDMSB-*b*-PMMA) deposited on a topographical varying substrate. The substrate surface has a rectangular wave shape with a period of 300 nm ($13.8L_0$), consisting of trenches that are 230 nm ($10.6L_0$) wide and 50 nm ($2.30L_0$) deep, separated by 70 nm ($3.23L_0$) wide mesas. The $C_\parallel$ orientation was obtained when the film thickness was 40 nm, while for film thickness of 30 nm the orientation $C_\perp$. This indicated that the perpendicular $C_\perp$ phase is more stable when decreasing the thickness of thin BCP films. For the confined di-BCP thin film, the effect of decreasing the film thickness is equivalent to increasing the roughness of the substrate. This was indeed shown by simulations of Vu et al.,[38] who demonstrated via SCFT calculation that the film thickness is a decreasing function of the mean curvature.

Furthermore, as can be seen in Figures 4b,d, for large u, increasing the substrate roughness results in a $C_\parallel^1$-to-$C_\parallel^2$ transition. Choi and co-workers[21] observed a similar phenomenon through changing the film thickness. They show scanning force microscopy (SFM) images of PS-*b*-poly(ethylene oxide) (PS-*b*-PEO) thin films on the minimal patterns. The minimal trench pattern consists of rectangular-waved substrate surface having a pitch of 139 nm ($6.35L_0$), a width of 99 nm ($4.52L_0$), and a depth of 15 nm ($0.68L_0$). As the film thickness increased from 22.6 to 41.0 nm, the cylindrical microdomains oriented from aligning parallel to

DOI: 10.1021/acs.macromol.8b02302
Macromolecules 2019, 52, 1241−1248

orthogonal to the trench direction ($C_{\parallel}^{2}$-to-$C_{\parallel}^{1}$). If the increase of film thickness can be thought of as reducing the substrate roughness, our findings qualitatively agree with those experimental findings.

Varying the preference of the substrate for the minority A component can also cause a phase transition between the three cylinder orientations. The $C_{\parallel}^{1}$ is more stable for large u values. Similar effects of u were reported by Man et al.[30,31] They showed that increasing u can cause a phase transition from perpendicular to parallel orientation of lamellar phases. This indeed indicates that for both the cylinder and lamellar morphologies the substrate preference u can cause a phase transition from the perpendicular to parallel orientation.

We illustrate, in addition, the relative stability of three cylinder orientations by comparing their free energies of the three orientations. The dependence of the corresponding free energies is shown in Figures 5 and 7. Our results demonstrate that the free energy is an increasing function of the substrate amplitude R. This is consistent with previous simulations,[38] which showed that the free energy is an increasing function of the substrate curvature. In another study, Peng et al.[29] studied the trend of the free energy by simulating BCP thin films on sawtoothed substrates. They obtained that the free energy decreases as the film thickness increases. The increase of film thickness decreases the fraction of nonflat substrate and is equivalent to a decrease of the substrate roughness.

It is worth to notice that such a lateral confinement can result in more complex patterns than the three defect-free cylindrical phases studied in the present work. A possible effect of the nonflat substrate is that it may induce melting of the cylindrical phases toward a poorly ordered phase. This will occur when the substrate roughness is large and its pattern periodicity is not an integer number of the natural periodicity of the cylinder lattice. Moreover, Peng et al.[29] showed that rich pattern conformations are obtained when the cylinders are in contact with a sawtoothed substrate by using SCFT calculations. It is clear that a full phase diagram of cylinder forming BCP thin film on a sinusoidal substrate can be very complicated. We leave this issue to a future study.

In conclusion, within the framework of SCFT we explored the influence of substrate roughness on the relative stability of three cylindrical BCP phases having different orientations. The impacts of the amplitude, periodicity, and surface preference on the cylinder orientations were studied only for conditions allowing to achieve defect-free BCP structures. Increasing the substrate roughness (increasing R or, separately, decreasing L_s) causes the cylindrical phase to have an orientation perpendicular to the substrate when the substrate preference parameter is moderate. Phase transitions from $C_{\perp}$ to $C_{\parallel}^{2}$ and from $C_{\parallel}^{2}$ to $C_{\parallel}^{1}$ are observed via increasing the substrate preference. We find that the perpendicular cylindrical phase is more stable when the substrate corrugations undulate along the larger b-direction rather than along the shorter a-direction. Our results are seemingly robust as they in agreement with several experimental results. In addition to the roughness and preference of substrate, there are several other parameters that can influence the orientation and relative stability of the cylindrical phase, for example, the film thickness, the relative preference of the top surface, and so forth. We hope that our results can become a useful guide for future experiments as well as for applications.

AUTHOR INFORMATION

Corresponding Author

*E-mail manxk@buaa.edu.cn.

ORCID

Karim Aissou: 0000-0002-9236-464X

David Andelman: 0000-0003-3185-8475

Xingkun Man: 0000-0003-4266-1539

Notes

The authors declare no competing financial interest.

ACKNOWLEDGMENTS

We thank A.-C. Shi and W. H. Li for useful discussions. This work was supported in part by Grants 21822302 and 21434001 of the National Natural Science Foundation of China (NSFC), the NSFC-ISF Research Program, jointly funded by the NSFC under Grant 51561145002, and the Israel Science Foundation (ISF) under Grant 885/15.

REFERENCES

(1) Bates, F. S.; Schulz, M. F.; Khandpur, A. K.; Förster, S.; Rosedale, J. H.; Almdal, K.; Mortensen, K. Fluctuations, conformational asymmetry and block copolymer phase behaviour. *Faraday Discuss.* **1994**, *98*, 7.

(2) Epps, T. H.; Cochran, E. W.; Bailey, T. S.; Waletzko, R. S.; Hardy, C. M.; Bates, F. S. Ordered Network Phases in Linear Poly(isoprene-b-styrene-b-ethylene oxide) Triblock Copolymers. *Macromolecules* **2004**, *37*, 8325.

(3) Li, W.; Liu, M. F.; Qiu, F.; Shi, A.-C. Phase Diagram of Diblock Copolymers Confined in Thin Films. *J. Phys. Chem. B* **2013**, *117*, 5280.

(4) Xie, N.; Li, W.; Qiu, F.; Shi, A.-C. σ Phase Formed in Conformationally Asymmetric AB-Type Block Copolymers. *ACS Macro Lett.* **2014**, *3*, 906.

(5) Bates, F. S.; Fredrickson, G. H. Block Copolymers: Designer Soft Materials. *Phys. Today* **1999**, *52*, 32.

(6) Cheng, J. Y.; Ross, C. A.; Chan, Z. H.; Thomas, E. L.; Lammertink, R. G. H.; Vancso, G. J. Formation of a Cobalt Magnetic Dot Array via Block Copolymer Lithography. *Adv. Mater.* **2001**, *13*, 1174.

(7) Jeong, S.-J.; Xia, G.; Kim, B. H.; Shin, D. O.; Kwon, S.-H.; Kang, S.-W.; Kim, S. O. Universal Block Copolymer Lithography for Metals, Semiconductors, Ceramics, and Polymers. *Adv. Mater.* **2008**, *20*, 1898.

(8) Yang, S. Y.; Ryu, L.; Kim, H. Y.; Kim, J. K.; Jang, S. K.; Russell, T. P. Nanoporous Membranes with Ultrahigh Selectivity and Flux for the Filtration of Viruses. *Adv. Mater.* **2006**, *18*, 709.

(9) Thurn-Albrecht, T.; Schotter, J.; Kastle, C. A.; Emley, N.; Shibauchi, T.; Krusin-Elbaum, L.; Guarini, K.; Black, C. T.; Tuominen, M. T.; Russell, T. P. Ultrahigh-density nanowire arrays grown in self-assembled diblock copolymer templates. *Science* **2000**, *290*, 2126.

(10) Peng, Q.; Tseng, Y.-C.; Darling, S. B.; Elam, J. W. A Route to Nanoscopic Materials via Sequential Infiltration Synthesis on Block Copolymer Templates. *ACS Nano* **2011**, *5*, 4600.

(11) Huang, E.; Rockford, L.; Russell, T. P.; Hawker, C. J. Nanodomain control in copolymer thin films. *Nature* **1998**, *395*, 757.

(12) Man, X. K.; Andelman, D.; Orland, H. Block copolymer films with free interfaces: Ordering by nanopatterned substrates. *Phys. Rev. E* **2012**, *86*, 010801.

(13) Morkved, T. L.; Lu, M.; Urbas, A. M.; Ehrichs, E. E.; Jaeger, H. M.; Mansky, P.; Russell, T. P. Local Control of Microdomain Orientation in Diblock Copolymer Thin Films with Electric Field. *Science* **1996**, *273*, 931.

(14) Kang, H.; Craig, G. S. W.; Han, E.; Gopalan, P.; Nealey, P. F. Degree of Perfection and Pattern Uniformity in the Directed Assembly of Cylinder-Forming Block Copolymer on Chemically Patterned Surfaces. *Macromolecules* **2012**, *45*, 159.

DOI: 10.1021/acs.macromol.8b02302
Macromolecules 2019, 52, 1241−1248

(15) Vega, D. A.; Gomez, L. R.; Pezzutti, A. D.; Pardo, F.; Chaikin, P. M.; Register, R. A. Coupling Between Mean Curvature and Textures in Block Copolymer Thin Films Deposited on Curved Substrates. *Soft Matter* **2013**, *9*, 9385.
(16) Zhang, L. S.; Wang, L. Q.; Lin, J. P. Harnessing anisotropic nanoposts to enhance long-range orientation order of directed selfassembly nanostructures via large cell simulations. *ACS Macro Lett.* **2014**, *3*, 712.
(17) Cong, Z. N.; Zhang, L. S.; Wang, L. Q.; Lin, J. P. Understanding the ordering mechanisms of self-assembled nano structures of block copolymers during zone annealing. *J. Chem. Phys.* **2016**, *144*, 114901.
(18) Sinturel, C.; Vayer, M.; Morris, V. M.; Hillmyer, M. A. Solvent Vapor Annealing of Block Polymer Thin Films. *Macromolecules* **2013**, *46*, 5399.
(19) Hong, S. W.; Voronov, D. L.; Lee, D. H.; Hexemer, A.; Padmore, H. A.; Xu, T.; Russell, T. P. Controlled Orientation of Block Copolymers on Defect-Free Faceted Surfaces. *Adv. Mater.* **2012**, *24*, 4278.
(20) Hong, S. W.; Huh, J.; Gu, X.; Lee, D. H.; Jo, W. H.; Park, S.; Xu, T.; Russell, T. P. Unidirectionally Aligned Line Patterns Driven by Entropic Effects on Faceted Surfaces. *Proc. Natl. Acad. Sci. U. S. A.* **2012**, *109*, 1402.
(21) Choi, J.; Li, Y.; Kim, P. Y.; Liu, F.; Kim, H.; Yu, D. M.; Huh, J.; Carter, K. R.; Russell, T. P. Orthogonally Aligned Block Copolymer Line Patterns on Minimal Topographic Patterns. *ACS Appl. Mater. Interfaces* **2018**, *10*, 8324.
(22) Tavakkoli, K. G. A.; Nicaise, S. M.; Gadelrab, K. R.; Alexander-Katz, A.; Ross, C. A.; Berggren, K. K. Multilayer Block Copolymer Meshes by Orthogonal Self-assembly. *Nat. Commun.* **2016**, *7*, 10518.
(23) Park, S.; Lee, D. H.; Xu, J.; Kim, B.; Hong, S. W.; Jeong, U.; Xu, T.; Russell, T. P. Macroscopic 10-Terabit-per-Square-Inch Arrays from Block Copolymers with Lateral Order. *Science* **2009**, *323*, 1030.
(24) Aissou, K.; Shaver, J.; Fleury, G.; Pecastaings, G.; Brochon, C.; Navarro, C.; Grauby, S.; Rampnoux, J.-M.; Dilhaire, S.; Hadziioannou, G. Nanoscale Block Copolymer Ordering Induced by Visible Interferometric Micropatterning: A Route towards Large Scale Block Copolymer 2D Crystals. *Adv. Mater.* **2013**, *25*, 213.
(25) Rho, Y.; Aissou, K.; Mumtaz, M.; Kwon, W.; Pecastaings, G.; Mocuta, C.; Stanecu, S.; Cloutet, E.; Brochon, C.; Fleury, G.; Hadziioannou, G. Laterally Ordered Sub-10 nm Features Obtained From Directed Self-Assembly of Si-Containing Block Copolymer Thin Films. *Small* **2015**, *11*, 6377.
(26) Kim, T.; Wooh, S.; Son, J. G.; Char, K. Orientation Control of Block Copolymer Thin Films Placed on Ordered Nanoparticle Monolayers. *Macromolecules* **2013**, *46*, 8144.
(27) Choi, J.; Huh, J.; Carter, K. R.; Russell, T. P. Directed Self-Assembly of Block Copolymer Thin Films Using Minimal Topographic Patterns. *ACS Nano* **2016**, *10*, 7915.
(28) Aissou, K.; Mumtaz, M.; Fleury, G.; Portale, G.; Navarro, C.; Cloutet, E.; Brochon, C.; Ross, C. A.; Hadziioannou, G. Sub-10 nm Features Obtained from Directed Self-Assembly of Semicrystalline Polycarbosilane-Based Block Copolymer Thin Films. *Adv. Mater.* **2015**, *27*, 261.
(29) Peng, M.; Ma, S.; Hu, J.; Wang, R. Hierarchical Nanostructures of Diblock Copolymer Thin Films Directed by a Saw-toothed Substrate. *Soft Matter* **2015**, *11*, 6642.
(30) Man, X. K.; Tang, J. Z.; Zhou, P.; Yan, D. D.; Andelman, D. Lamellar Diblock Copolymers on Rough Substrates: Self-Consistent Field Theory Studies. *Macromolecules* **2015**, *48*, 7689.
(31) Man, X. K.; Zhou, P.; Tang, J. Z.; Yan, D. D.; Andelman, D. Defect-Free Perpendicular Diblock Copolymer Films: The Synergy Effect of Surface Topography and Chemistry. *Macromolecules* **2016**, *49*, 8241.
(32) Carpenter, C. L.; Nicaise, S.; Theofanis, P. L.; Shykind, D.; Berggren, K. K.; Delaney, K. T.; Fredrickson, G. H. Orientational Preference in Multilayer Block Copolymer Nanomeshes with Respect to Layer-to-Layer Commensurability. *Macromolecules* **2017**, *50*, 8258.
(33) Matsen, M. W. Thin Films of Block Copolymer. *J. Chem. Phys.* **1997**, *106*, 7781.
(34) Bosse, A. W.; García-Cervera, C. J.; Fredrickson, G. H. Microdomain Ordering in Laterally Confined Block Copolymer Thin Films. *Macromolecules* **2007**, *40*, 9570.
(35) Hur, S.-M.; García-Cervera, C. J.; Kramer, E. J.; Fredrickson, G. H. SCFT Simulations of Thin Film Blends of Block Copolymer and Homopolymer Laterally Confined in a Square Well. *Macromolecules* **2009**, *42*, 5861.
(36) Takahashi, H.; Laachi, N.; Delaney, K. T.; Hur, S.-M.; Weinheimer, C. J.; Shykind, D.; Fredrickson, G. H. Defectivity in Laterally Confined Lamella-Forming Diblock Copolymers: Thermodynamic and Kinetic Aspects. *Macromolecules* **2012**, *45*, 6253.
(37) Matsen, M. W. Effect of Architecture on the Phase Behavior of AB-type Block Copolymer Melts. *Macromolecules* **2012**, *45*, 2161.
(38) Vu, G. T.; Abate, A. A.; Gómez, L. R.; Pezzutti, A. D.; Register, R. A.; Vega, D. A.; Schmid, F. Curvature as a Guiding Field for Patterns in Thin Block Copolymer Films. *Phys. Rev. Lett.* **2018**, *121*, 087801.

NOTE ADDED AFTER ASAP PUBLICATION

Due to a production error, this paper was published ASAP on January 30, 2019, without the final corrections applied. The corrected version was reposted on February 4, 2019.

DOI: 10.1021/acs.macromol.8b02302
Macromolecules 2019, 52, 1241−1248